A STUDY OF THE EFFECT OF GEOMAGNETIC FIELD ON EXTENSIVE AIR SHOWERS WITH SMALL ARRAYS

M. BAHMANABADI[1*], A. ANVARI[1], M. KHAKIAN GHOMI[1], D. PURMOHAMMAD[1], J. SAMIMI[1] and M. LAMEHI RACHTI[2]
[1] *Physics Department, Sharif University of Technology, Tehran, Iran;*
[2] *Van de Graaf Laboratory, Aeio, Tehran, Iran*
(author for correspondence, e-mail: bahmanabadi@sina.sharif.ac.ir)*

(Received 3 April 2001; accepted 19 November 2002)

Abstract. We have studied Extensive Air Showers (EAS) with two small arrays of 1 m^2 scintillation detectors in Tehran, 1200 m above sea level.The distribution of air showers in zenith and azimuth angles has been studied and a $\cos^n \theta$ distribution with $n = 7.2 \pm 0.2$ was obtained for zenith angle distribution. An asymmetry has been observed in the azimuthal distribution of EAS of cosmic rays because of magnetic field of the Earth. Amplitudes of the first and the second harmonics of observed distribution depend on zenith angle as $A_I \approx (0.02 + 0.35 \sin^2 \theta) \pm 0.02$, and $A_{II} \approx (0.03 + 0.42 \sin^4 \theta) \pm 0.03$. Meanwhile, the uncertainties arising from the instrument, transit location of shower particles in the scintillator and fluctuations in the shower front have been calculated.

Keywords: cosmic rays, Extensive Air Shower, geomagnetic field

1. Introduction

The ultra high energy (UHE) cosmic rays having energies greater than 100 TeV are usually observed by detection of their air showers. The shower itself is detected by a surface array of detectors which usually consist of several scintillator detectors and sometimes other types of particle detectors for improvement of accuracy. The arrival direction of an air shower can be determined from fast timing data of the detectors and hence the accuracy of the obtained direction depends on the accuracy of time measurements. The detectors can also determine the local density of shower particles. In this article we are concerned only with scintillation detector arrays. Each detector is formed by an enclosure with reflective interior surface housing the plastic scintillator and one or more photomultiplier tubes (PMTs) viewing it. An air shower array with 1 m^2 scintillation detectors has been constructed in Tehran (35°43′N, 51°20′E). The elevation of the site is 1200 m above sea level (890 g cm^{-2}). The purposes of the experiment are as follows:

1. Estimation of the effect of uncertainty in time of CR crossing on angular resolution; to estimate the uncertainty of the CR arrival time measurements due to the light enclosures.

Experimental Astronomy **13:** 39–57, 2002.
© 2003 *Kluwer Academic Publishers. Printed in the Netherlands.*

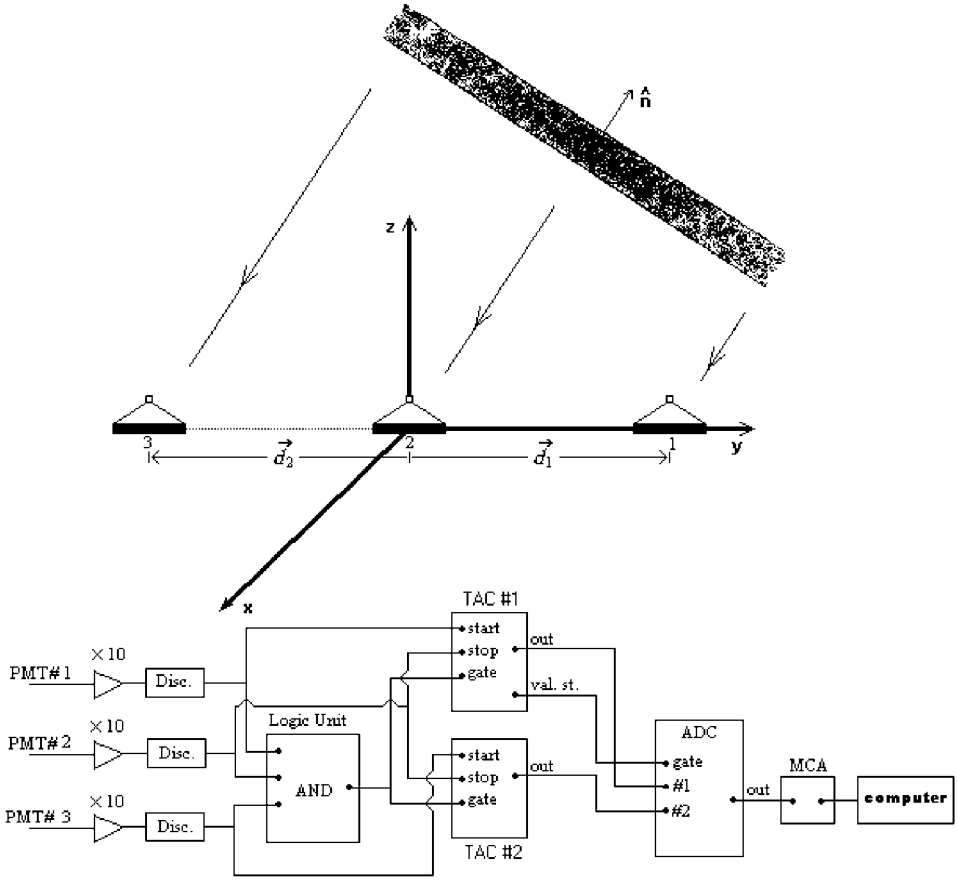

Figure 1. Schematic diagram of triple array and its electronic circuit.

2. Determination of zenith angle distribution of air showers at site level.
3. Investigation of the Earth's magnetic field effect on the azimuthal distribution of EAS of cosmic rays.

This experiment is the first step toward construction of an EAS array on Alborz mountain range at an altitude of over 2500 m near Tehran.

2. Experimental arrangements

The block diagram of electronic apparatus and detectors is shown in Figure 1. Three large area ($100 \times 100 \times 2$ cm^3) plastic scintillators were used both to detect the air showers and to record the arrival time of the particles. Each scintillator was enclosed in a pyramidal light enclosure of 15 cm height with white painted walls (Bahmanabadi et al., 1998) and a 5 cm diameter PMT (EMI9813KB) at the vertex

of the light enclosure. Signals from the PMTs are amplified in one stage ($\times$ 10) with a fast amplifier (CAEN N412). Then the signals are connected to an 8-channel fast discriminator (CAEN N413A) which was operated in fixed level of 20 mV. Each channel of the discriminator has two outputs; one of them is connected to a logic unit (CAEN N405) with a gate width of 150 ns, and the other to a TAC (ORTEC 566), so that the output of the scintillators Nos. 1 and 3 are connected to start input of the TAC Nos. 1 and 2, respectively, and output of the scintillator No. 2 is connected to the stop input of both TACs. Then the output of both TACs which were set to a full scale of 200 ns are fed into a multi-channel analyzer (MCA) via an analog to digital converter (ADC) unit. The triggering of the apparatus was made, when the three scintillators are fired. When triggering condition was confirmed by logic unit, the time lags between the output signals of scintillators 1 and 2, and 2 and 3 are read out by a computer. Two arrangements were used for this experiment. In Arrangement I, three scintillators lie on top of each other with separation of 70 cm, so that most of the triple coincidences are due to travel of a single muon. In Arrangement II, the three scintillators were layed on a horizontal line 510 cm apart (see Figure 1). Coincidences of the Arrangement II (Linear arrangement) are due to extensive air showers.

A second experiment was carried out with four scintillators as a square array which is shown in Figure 2. The block diagram of the circuit for data taking is also shown in the figure. When the four scintillators were fired, the apparatus is triggered by a logic unit with a 150 ns gate width , and time lags between the output signals of PMTs (1,4), (3,4), and (2,3) are read out by a computer.

3. Data analysis method

In Figure 1 we have shown an 'instantaneous profile' of a shower about to strike the scintillators. Individual shower particles are represented by dots. In our analysis, we assume the front surface of an air shower disk is approximately a plane perpendicular to the direction of the primary cosmic ray. Let a unit vector $\hat{n}$ represent the incident direction of the air shower, which in xyz coordinate system is:

$$\hat{n} = \sin\theta\cos\phi\hat{i} + \sin\theta\sin\phi\hat{j} + \cos\theta\hat{k} \,, \tag{1}$$

where, θ and ϕ are zenith and azimuth angles, respectively. We define T_{21} to be the time lag between pulses 1 and 2 and T_{23} between pulses 2 and 3. If we measure T_{21} and T_{23} from three scintillators, we can determine the arrival direction, $\hat{n}$. In order to interpret the experimental data we require expressions for T_{21} and T_{23} involving the geometrical properties of showers that we wish to measure, and take into account the thickness of the shower disks and the instrumental fluctuations:

$$T_{21} = \frac{1}{c}\vec{d}_1\cdot\hat{n} + (T_2 - T_1) + (\tau_2 - \tau_1) + (t_2 - t_1) \,, \tag{2}$$

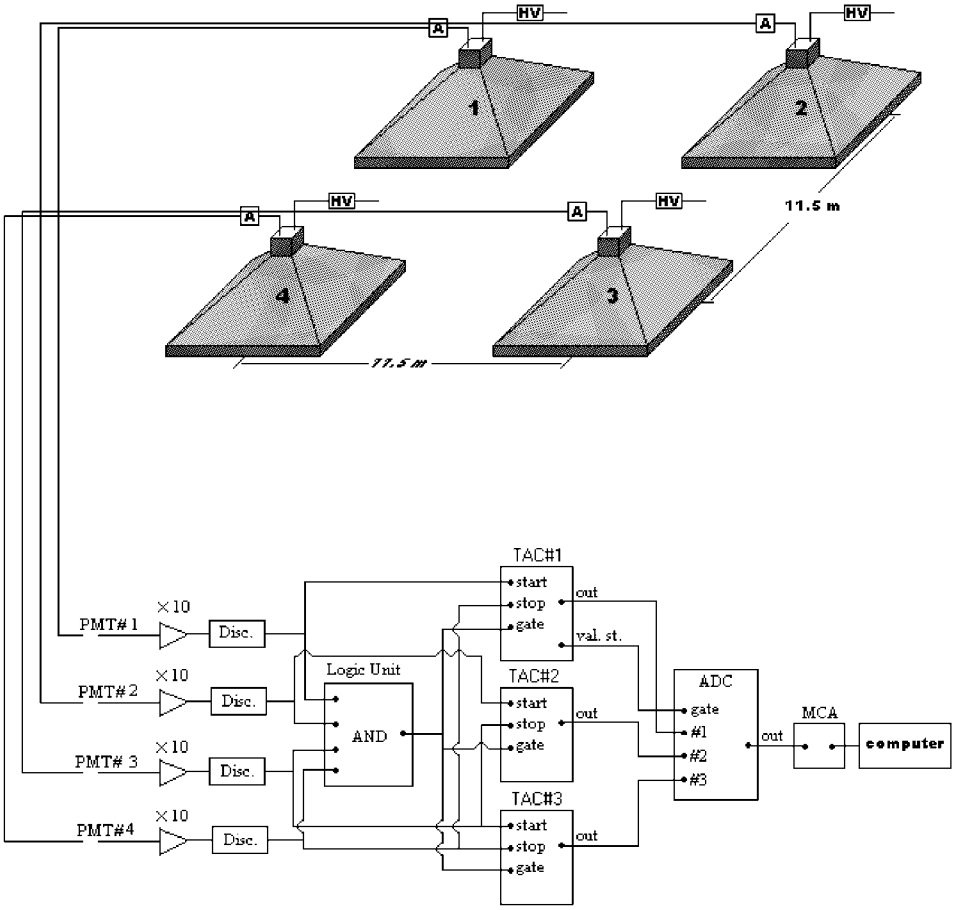

Figure 2. Schematic diagram of four detector array and its electronic circuit.

$$T_{23} = \frac{1}{c}\vec{d}_2 \cdot \hat{n} + (T_2 - T_3) + (\tau_2 - \tau_3) + (t_2 - t_3) \ , \tag{3}$$

the differences in the arrival times of the front at the various scintillators due to axis orientation are represented by terms involving $\vec{d}_1$ and $\vec{d}_2$, the position vectors of the scintillators (Figure 1). We assume all particles have velocity of light, c. T_1, T_2, and T_3 are the fixed delays artificially introduced for display purposes. τ_1, τ_2 and τ_3 represent the random instrumental errors, and t_1, t_2, and t_3 are the differences between the arrival times of the front at the three scintillators and the actual arrival times of the first particle at the scintillators. In the following discussion we use the statistical concept of dispersion of a variable x which is denoted by $D(x)$. We assume in our analysis that the instrumental fluctuations are the same for all three pulses, i.e.,

$$D(\tau_1) = D(\tau_2) = D(\tau_3) = D(\tau) \ . \tag{4}$$

In the case of Arrangement I, T_{12} and T_{23} are:

$$T_{21} = \frac{d/\cos\theta}{c} + (T_2 - T_1) + (\tau_2 - \tau_1) \,, \tag{5}$$

$$T_{23} = \frac{-d/\cos\theta}{c} + (T_2 - T_3) + (\tau_2 - \tau_3) \,, \tag{6}$$

where d is the distance between scintillators. As mentioned earlier, most of the coincidences with Arrangement I are produced by downward moving single muons. Thus there is no term involving t in Equations (5) and (6). If Equations (5) and (6) are added then,

$$T_{21} + T_{23} = (2T_2 - T_1 - T_3) + (2\tau_2 - \tau_1 - \tau_3) \,. \tag{7}$$

From Equations (4) and (7) we have

$$D_I(\tau) = \frac{1}{6}\left[D_I\,(T_{21} + T_{23})\right] \,. \tag{8}$$

Subscript on the symbol D indicates the experimental arrangement. For the Arrangement II the difference between the arrival time of the shower front and the actual arrival time of the first particle at a particular scintillator does not depened on the location of the scintillator. Thus, we may safely assume,

$$D(t_1) = D(t_2) = D(t_3) = D(t) \,. \tag{9}$$

Thus if the arrangement lays on y axis in xyz coordinate system (Figure 1) we have

$$T_{21} = +\frac{d}{c}\sin\theta\sin\phi + (T_2 - T_1) + (\tau_2 - \tau_1) + (t_2 - t_1) \,, \tag{10}$$

$$T_{23} = -\frac{d}{c}\sin\theta\sin\phi + (T_2 - T_3) + (\tau_2 - \tau_3) + (t_2 - t_3) \,. \tag{11}$$

Adding Equations (10) and (11) and considering Equations (4) and (9) we find

$$D_{II}(T_{21} + T_{23}) = 6D_{II}(\tau) + 6D(t). \tag{12}$$

Thus from Equation (12):

$$D_{II}(\tau) = \frac{1}{6}D_{II}(T_{21} + T_{23}) - D(t) \,. \tag{13}$$

Where $D(t)$ is the dispersion of times of first electron arrival, averaged over shower sizes and over distances from shower axis. $c[D(t)]^{1/2}$ is an indication of the mean thickness of the shower disks.

TABLE I
Specifications of experiments with Arrangements I and II

Arrangement	No. of events	$\sqrt{D(T_{21}+T_{23})}$ (ns)	Exposure time (s)
I	77000	3.8±0.01	15000
II	7530	9.3±0.08	72000

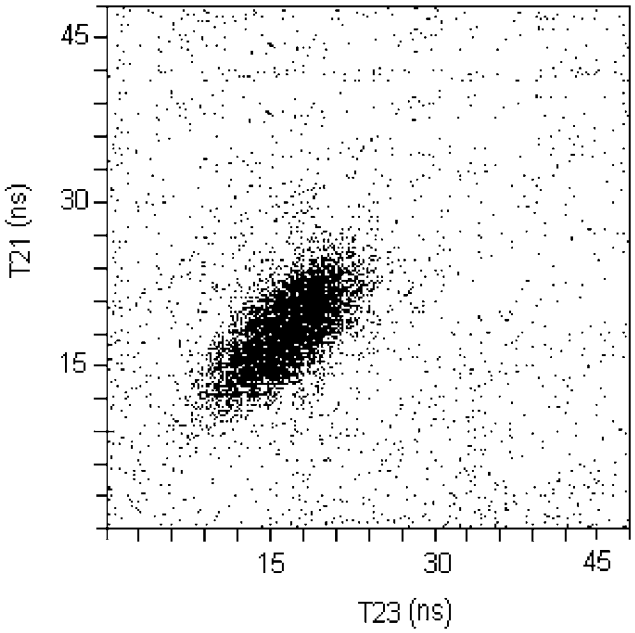

Figure 3. Time distribution of extensive air showers with Arrangement II.

4. Experimental measurements and results

4.1. Determination of thickness of shower disk and instrumental fluctuations

Figure 3 shows a way of plotting the experimental data which clarifies the statistical problems involved in the analysis. We recorded a large number of shower events with a certain disposition of scintillators, and for each event we obtained T_{21} and T_{23}. Each event is then represented by a point with cartesian coordinates T_{21} and T_{23}. In this plot the points for a typical experimental run with Arrangement II are distributed in an approximately elliptical region whose major axis is inclined at 45° and the points distributed uniformly represent random coincidence events. In order to demonstrate the interpretation of the rather uniformly distributed points we have performed several random coincidence runs. In these runs the muon events

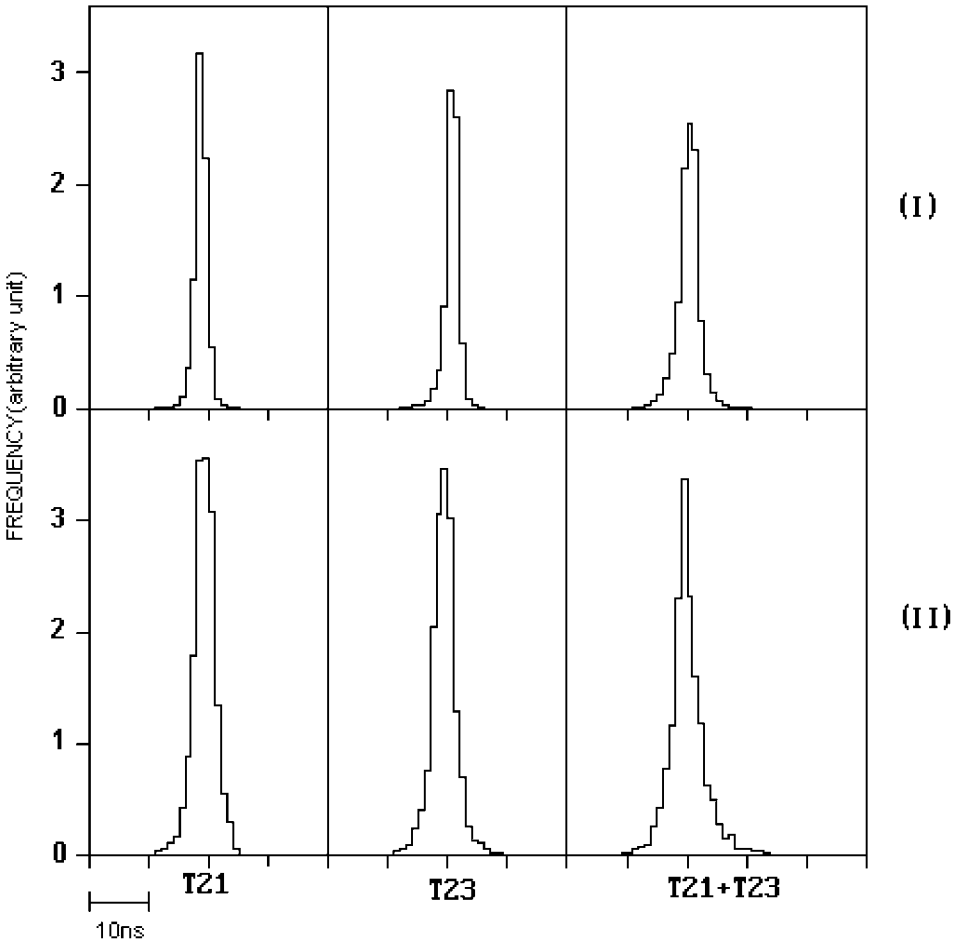

Figure 4. Histogram of T_{21}, T_{23}, and $T_{21}+T_{23}$. The scale on the horizontal axes is 10 ns per division.

(Arrangement I) and the shower events (Arrangement II) were delaberately omitted by manipulating the fixed time delays. The results of these runs are uninteresting plots showing points merely distributed uniformly and they are not shown here for brevity. Note that if $T_2 - T_1 \neq T_2 - T_3$, the major axis does not pass through the origin. From Equation (12) it is clear that the breadth of elliptical region is mostly related to the thickness of the shower disks. The distribution of points on the axis is related to the distribution of zenith and azimuth angles of shower axes (Equations (10) and (11)). The points out of the dense region are random events. In Figure 3 the projected distributions of points on the horizontal and vertical axes and the 45° line represent T_{21}, T_{23} and $\frac{1}{\sqrt{2}}(T_{21}+T_{23})$ distributions, respectively. Figure 4 shows histograms of T_{21}, T_{23} and $T_{21}+T_{23}$ obtained with various arrangements. In Table I we have listed the values of $[D(T_{21}+T_{23})]^{\frac{1}{2}}$ and the numbers of events used

in the calculations. The dispersion due to instrumental fluctuations is calculated by Equation (8). This fluctuations arise partly from fluctuating delays in the light enclosure of scintillators and electronic circuits. assuming the dispersions of τ_1, τ_2 and τ_3 to be equal, we find

$$[D_I(\tau)]^{1/2} = \left[\frac{1}{6} D_I\,(T_{21} + T_{23})\right]^{1/2} = 1.5\text{ns}\ . \tag{14}$$

The error in arrival time can be represented as $[\sigma^2_{elec.} + \sigma^2_{L.E.}]^{1/2}$, where $\sigma_{elec.}$ and $\sigma_{L.E.}$ are the errors in time due to the electronic circuits, and light enclosure of scintillators, respectively. The error due to the light enclosure is 1.1 ns, according to our previous results (Bahmanabadi et al., 1998) for the passage of single muons through the scintillator. Then the rest of errors is due to the electronic circuits, that is 1 ns.

We can not a priori assume that the dispersion in τ for the two arrangements is the same. In Arrangement I single muons are crossing the scintillators, whereas in Arrangement II it is the electrons of EAS which are crossing. Generally, single muons produce much larger signals in scintillators than electrons. This will effect the characteristics of the electronic circuits. Also a single muon will produce light originating from a single line in the scintillator which will effect the time spreading of the light in the detector.

In order to estimate $D_{II}(\tau)$ from Equation (13), we need to have an estimate of the mean time dispersion due to the thickness of the shower disks in Arrangement II, $D(t)$. To this end, we have used the CORSIKA Code (Heck et al., 1998) to simulate showers generated by proton primaries of different zenith and azimuth angles. Each simulated shower with its core chosen randomly with respect to our array has been first checked for matching the trigger logic of detection by our array. For showers matching the trigger logic the dispersion in arrival times of the shower particles crossing each of the detectors of the array has been computed. The composite results of these computations for the simulated showers is shown in Figure 5. Here each point represent the mean value for 400 random choices of the shower core coordinates. In Figure 5a square root of the mean dispersion is displayed as a function of the primary zenith angle, in Figure 5b as a function of primary azimuth angle and in Figure 5c as a function of the number of the charged particles in the shower. The smooth curves are best fitted curves to the simulated data and represent rather useful information: (1) As expected, aside from shower-to-shower fluctuations, the dispersion in arrival times of the shower particles do not depend on the primary azimuth angle. However, (2) the mean dispersion gently decreases with increasing primary zenith angle, and (3) it gently increases with increasing number of the particles in the shower.

The distribution of the mean-square-root dispersions for our simulated set of showers is histogrammed in Figure 6. This distribution aside from showing a deficit in the last bins (large dispersions) which is attributed to the incompleteness of our

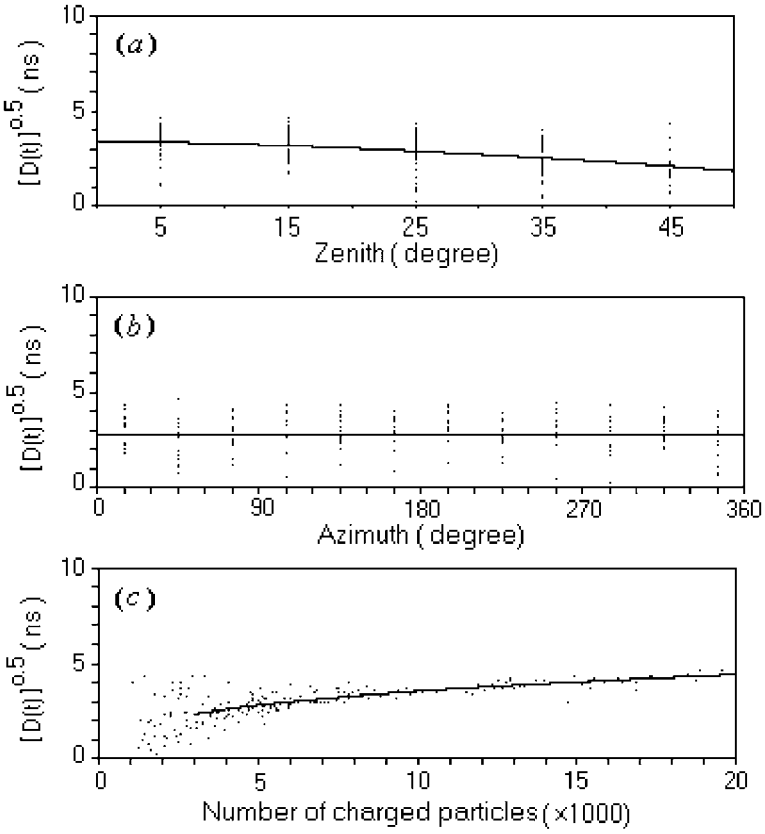

Figure 5. Mean-square-root of dispersion in arrival times of the shower particles crossing each detector, using CORSIKA code and the trigger logic for the square array, as a function of the (a) primary zenith angle, (b) primary azimuth angle, and (c) the number of charged particles in the shower.

simulated set at large number of shower particles, fits rather well to a guassian distribution which is represented by the smooth curve. We take the mean of this fitted guassian distribution as the best estimate of the overall mean-square-root dispersions in arrival times of the shower particles crossing each of the detectors in our experimental Arrangement II, $[D(t)]^{1/2}$. From Figure 6, we have $[D(t)]^{1/2} = 3.2$ ns. We also get $c[D(t)]^{1/2} = 0.96$ m as the best estimate of the mean thickness of the shower disks for the set of simulated showers used in our analysis.

Using the above value for $[D(t)]^{1/2}$, along with the dispersion in experimental timing data given in Table I, we can use Equation (13) to obtain $[D_{II}(\tau)]^{1/2} = 2$ ns. We see that this result is rather close to the 1.5 ns obtained for Arrangement I, Equation (14). We also see that $D_{II}(\tau) > D_I(\tau)$, which is due to the fact that in air shower experiments the detection process is dominated by signals close to threshold, whereas single muons in Arrangement I produce larger signals.

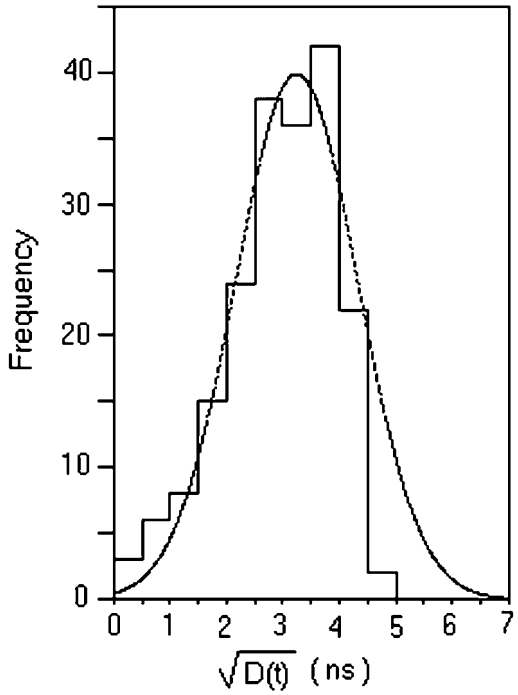

Figure 6. Distribution of the mean-square-root of dispersions in arrival times of the simulated shower particles crossing each detector. The smooth curve is a guassian fit to the distribution with a mean of 3.2 ns.

4.2. Effect of temporal and spatial errors on angular resolution

Now, if the time of arrival of the first shower particles detected in two adjacent scintillators of an EAS array separated by a distance d are s_1 and s_2, neglecting the curvature of shower front, the direction of the two parallel shower particles, $\hat{n}$, is obtained from the following simple relation (Figure 1)

$$\sin\theta \sin\phi = \frac{c}{d}(s_2 - s_1) \ . \tag{15}$$

The incident cosmic rays direction has approximately an axial symmetry (Bertou et al., 2000). Assuming that the errors in θ and ϕ are equal, we can therefore write the errors in θ as,

$$\Delta\theta = \sqrt{2}\left[2\left(\frac{c}{d}\Delta s\right)^2 + \frac{1}{2}\left(\frac{\Delta d}{d}\right)^2 \sin^2\theta\right]^{1/2} \ , \tag{16}$$

where $< \cos^2\phi >=< \sin^2\phi >= \frac{1}{2}$ has been used instead of $\sin^2\phi$ and $\cos^2\phi$, and Δs and Δd are the errors in determination of time of arrival and distance of

separation of the two shower particles. The errors in arrival time can be written as $\Delta s = \left[\sigma_i^2 + \sigma_{sh}^2\right]^{1/2}$, where $\sigma_i = [D_{II}(\tau)]^{1/2} = 2$ ns is the inherent uncertainty in time measurement and σ_{sh} is the variance in time of arrival of shower particles of a given detector due to the thickness of the EAS disk. Our measurements show that σ_{sh} is greater than σ_i. From Equation (1) of Linsley (1986) which parameterizes the shower thickness as a function of the distance of the detector from the shower core (r), we find the following expression for σ_{sh},

$$\sigma_{sh} = (1.6 \text{ ns})(1 + r/30)^{1.65}/\sqrt{n(r,\theta)}\,, \tag{17}$$

where r is in meters, and $n(r,\theta)$ is the number of shower particles crossing the detector located at a distance r from the core of a shower with zenith angle θ. For a 1 m^2 detector $n(r,\theta)$ is simply the shower particle density given by famous NKG formula. We have neglected the slight dependence of Equation (17) on zenith angle (Linsley, 1986). Thus Equation (16) is rewritten as

$$\Delta\theta = \sqrt{2}\left\{2\left(\frac{c}{d}\right)^2\left[\sigma_i^2 + 2.56\,(1 + r/30)^{3.3}/n(r)\right] + \frac{1}{2}\left(\frac{\Delta d}{d}\right)^2 \sin^2\theta\right\}^{1/2} \tag{18}$$

Equation (18) shows that for large values of r the error due to shower thickness is the dominant term. However, near the shower core the inherent timing error (σ_i) is larger than the error due to shower thickness (σ_{sh}). Specifically, for 1 m^2 detectors separated by 15 m, and a zenith angle of 20°, a typical shower may have a particle density of 50 at the core and thus we obtain $\Delta\theta = 4.8°$. For this example, the three error factors contributing to $\Delta\theta$, i.e., inherent timing error, shower thickness, and location uncertainty, will be, 4.6°, 0.5°, and 1.3°, respectively.

4.3. SQUARE ARRAY

With arrangement of four scintillators as a square array (Figure 2), we measured the time lag between the detectors (1,4), (3,4), and (2,3) for each shower. The time lags are represented by T_{14}, T_{34}, and T_{23}, respectively. Figure 7 shows a plot of T_{34} vs. T_{14} for a large number of showers. Since three scintillators 1, 3 and 4 have been placed at the vertices of a right triangle, the experimental points representing showers are distributed in a circular region whose center of gravity corresponds to a vertical shower. The points distributed uniformly represent random coincidence events as discussed in Section 4.1. The plot is actually a representation of angular distribution of shower axis direction. The azimuth and zenith angle of each shower axis can therefore be determined directly from the plot. An annular ring with radii S_a and S_b contains points representing shower axes with zenith angles in the range $\sin^{-1}(S_a c/d) < \Theta < \sin^{-1}(S_b c/d)$. If one measures the frequency of counts within successive annular rings, one can determine the distribution in zenith angle of shower axes. Figure 8a is a histogram of the zenith angle computed from Figure 7 by counting the points within successive annular rings. The differential zenith

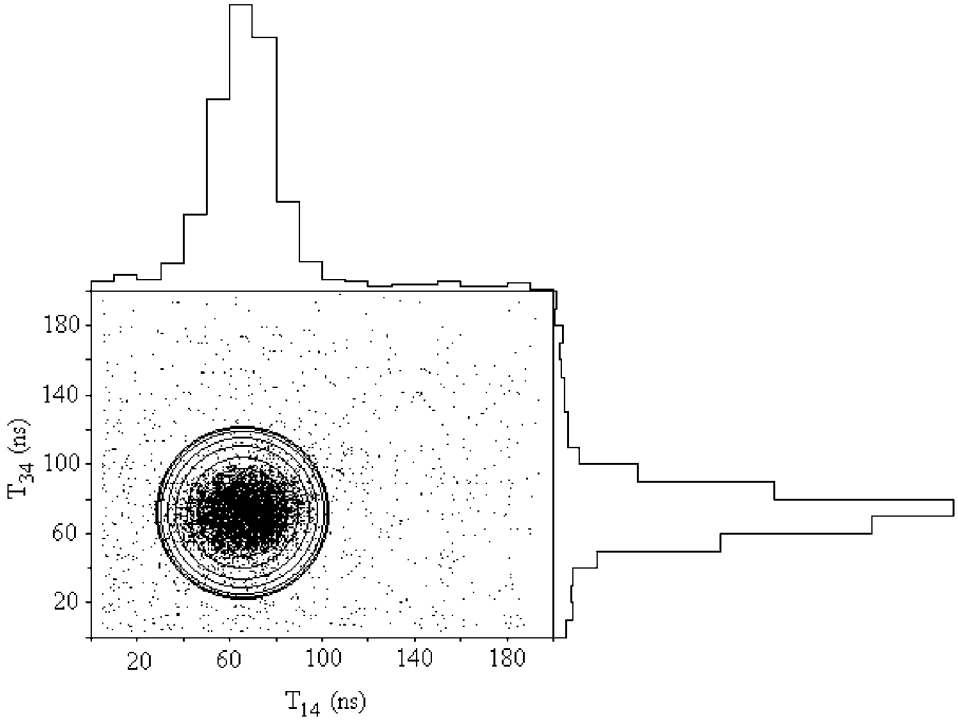

Figure 7. A plot of time lag distributions, T_{34} vs. T_{14} with square array.

angle distribution can be represented by $Z(\theta)d\theta = constant.\sin\theta\cos^n\theta d\theta$. We find $n = 7.6\pm0.2$ for this fit in the present apparatus at Tehran level. If the circles on Figure 7 are divided into sectors, one can determine the azimuthal distribution of EAS of cosmic rays by counting the points within each sector. In this method we use only two time lags i.e, T_{34} and T_{14}. Arrival direction of an air shower can also be determined by least-square method (Mitsui et al., 1990; Nishizawa et al., 1989). In the latter method three time lags, that is, T_{14}, T_{34}, and T_{23} are used for finding direction of each shower axis. Accuracy of the latter method is more than that of the former one. The formula used in calculations are given in the appendix. A set of about 14 000 showers was used for this analysis. Figure 8b shows the distribution of zenith angle, that has been obtained by least-square method. The exponent n is also calculated: $n = 7.2\pm0.2$. The exponent n increases as the shower size N or altitude decreases, so that its value at sea level for the range of relatively small showers ($6\times10^4 \leq N \leq 5\times10^5$) is $n = 10.0$ (Luorui and Winn, 1984).

Figure 9 shows the azimuthal distribution of EAS events with zenith angle in bins $5^\circ - 20^\circ$, $20^\circ - 35^\circ$, $35^\circ - 50^\circ$, and all zenith angles. The total number of EAS events in the zenith angle intervals used in the analysis has been given at the left side in Figure 9. The azimuth distribution shows a north-south asymmetry. This asymmetry was also seen for events above 5×10^{16} eV with the Yakutsk array

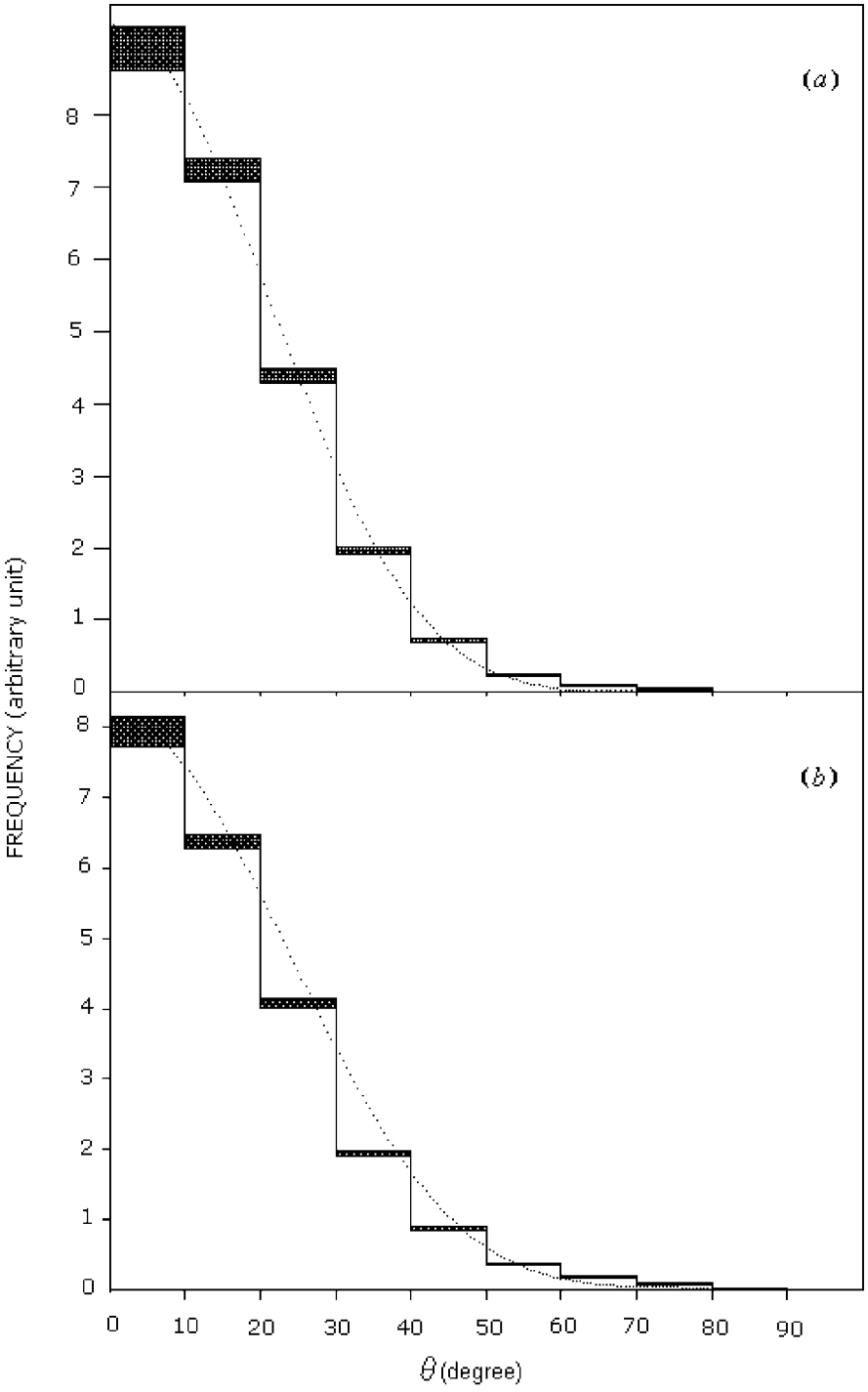

Figure 8. Frequency of showers per solid angle vs. zenith angle, θ. Distributions were obtained from data on Figure 7 (upper panel) and by least square method (lower panel). The shaded areas in the histograms show counting errors and dotted lines show the distribution function $\cos^n \theta$ (see the text).

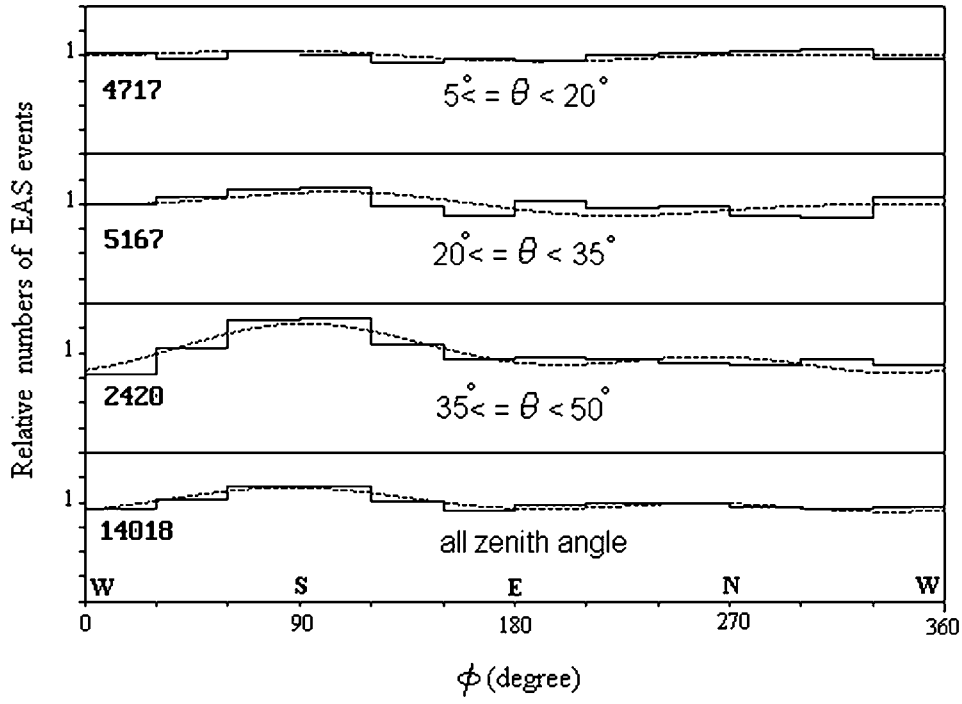

Figure 9. Relative numbers of EAS events in various zenith angle intervals (shown at each panel). Dotted lines show the ASYM function (see the text).

(Ivanov et al., 1999). In order to demonstrate that this north-south asymmetry is not due to the geometry of our square array we have repeated the experiment with the array rotated by 45°. The azimuth distributions for this experiment shown in Figure 10 exhibit a similar asymmetry. This shows that the effect stays fixed in space which in turn provides strong evidence for a geomagnetic origin.

We have also used showers simulated by CORSIKA code to obtain a rather similar azimuthal distribution. The values of geomagnetic field components for Tehran ($B_x = 28.06\mu$T, $B_z = 38.37\mu$T) were obtained from U.S. Geomagnetic Data Center (see internet address in Refs. 2002). The results for simulated showers is shown in Figure 11. The distributions in Figures 9 and 10 have been fitted to the following function:

$$ASYM = 1 + A_I \cos(\phi - B) + A_{II} \cos(2\phi - C) \; . \tag{19}$$

All fit parameters are shown in Table II. The values for A_I are almost always greater than A_{II}, that is the first harmonics are more important in the array region with the geomagnetic field zenith angle $\theta_H = 38°$. For other arrays the situation may be different. For example, at the Tibet array (30.11°N, 90.53°E) where the field zenith angle is $\theta_H = 45°$, both the first and the second harmonics are equally prevailing. At the Yakutsk array (62°N, 130°E; $\theta_H = 14°$) the first harmonic, and at

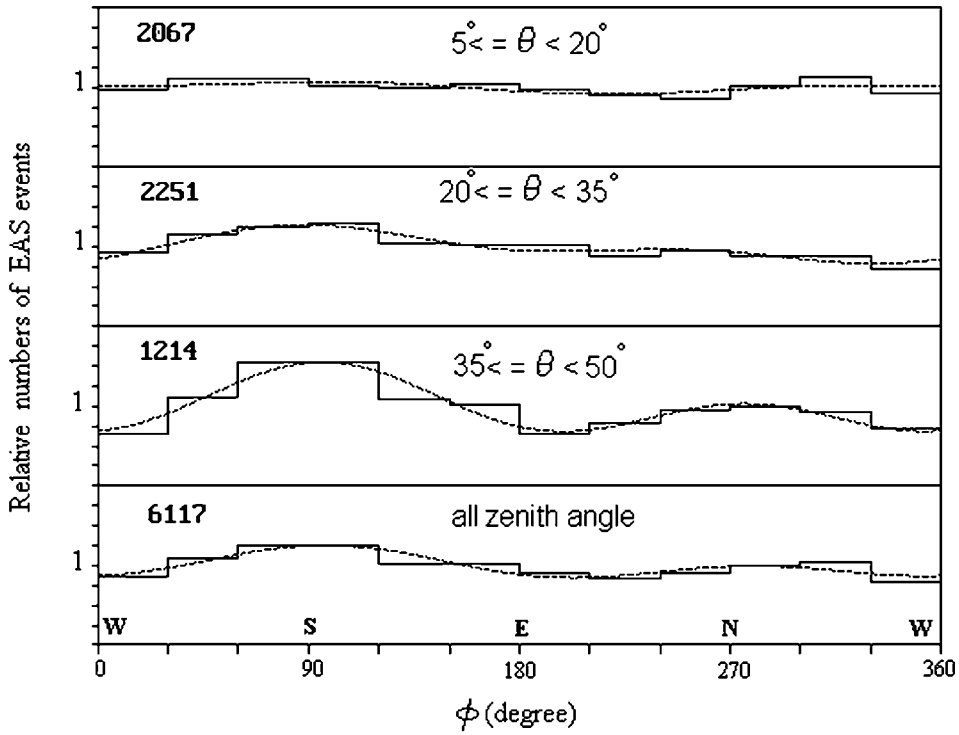

Figure 10. Same as Figure 9 for the experiment with square array rotated 45 degrees.

the Chakaltaya array (16.35°S, 68.2°W; $\theta_H = 88°$) the second harmonic dominate (Ivanov et al., 1999).

TABLE II

Coefficients of the function ASYM which were fitted to the data

Array		$5° \leq \theta < 20°$	$20° \leq \theta < 35°$	$35° \leq \theta < 50°$	$0° \leq \theta < 90°$
Original	A_I	0.0356	0.090	0.174	0.081
	A_{II}	0.0279	0.0488	0.1293	0.069
	B	35°	78°	103°	95°
	C	184°	234.5°	176.8°	–193°
45° Rotated	A_I	0.058	0.178	0.258	0.131
	A_{II}	0.032	0.109	0.288	0.124
	B	54°	107°	96°	93°
	C	240°	160°	192°	–164°

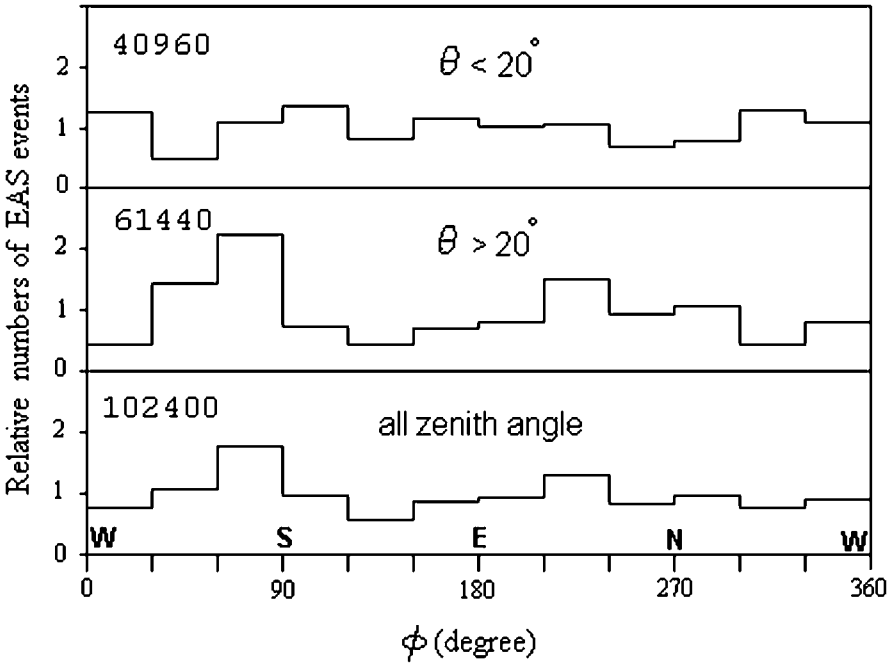

Figure 11. Azimuthal distribution of simulated showers generated by CORSIKA code with the geomagnetic field values of Tehran. The number of simulated showers has been given at the left side.

TABLE III

Comparison of overall south-north asymmetry of our two experiments and that of simulated showers generated by CORSIKA Code[$(N_s - N_n)/(N_s + N_n)$ (in %)]

Array	$5^\circ \leq \theta < 20^\circ$	$20^\circ \leq \theta < 35^\circ$	$35^\circ \leq \theta < 50^\circ$	$0^\circ \leq \theta < 90^\circ$
Original	7	13	18	12
45° Rotated	3	11	16	9
Both	6	12.4	17.3	11
Simulation	2	5	5	3.5

Using the amplitude of $(N_s - N_n)/(N_s + N_n)$, where $N_s(N_n)$ is the number of showers from south (north) half-space, as a function of zenith angle, we have compared the results of our two experiments (Original and 45° rotated) and that of the simulated showers in Table III for different zenith angle ranges. As a rule the asymmetry increases with increasing zenith angle. This is shown in Figure 12 where we have also compared our results (solid circles) with data of Yakutsk array (squares). As it is seen from this figure, the asymmetry amplitude increases

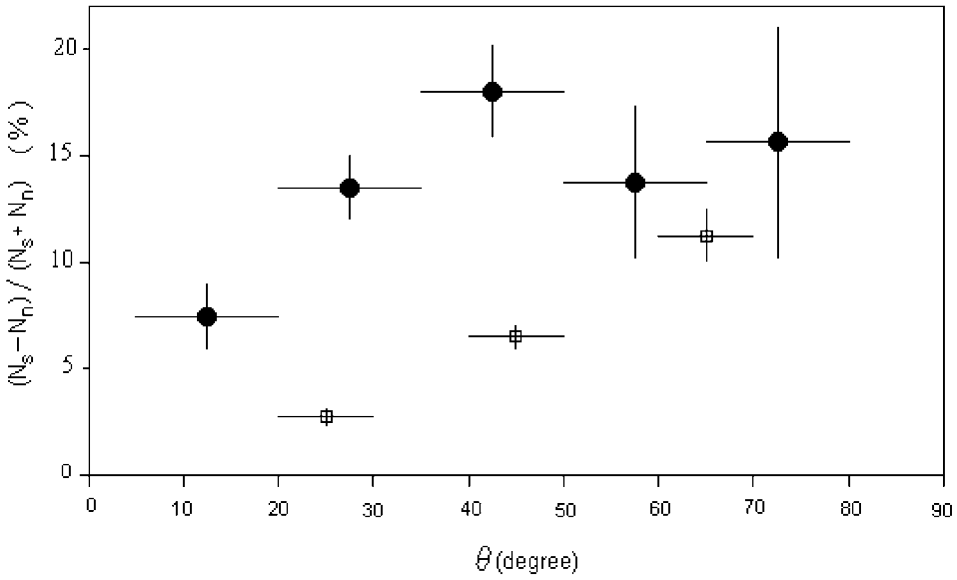

Figure 12. Relative difference of number of showers from south and north half space as a function of zenith angle. Our results (solid circles) have been compared with data of Yakutsk array (squares).

with θ. Also in our case this amplitude is more than Yakutsk results, because the geomagnetic field zenith angle in our site is greater than the one in Yakutsk.

5. Conclusion

The arrival direction of air showers are usually estimated by fast timing shower detection with scintillator arrays. Each scintillator is usually enclosed by a light enclosure. We have estimated uncertainties in time of arrival of a shower particle. These uncertainties are due to the shower thickness, the unknown position of transit in the large area scintillator, and the equipment, i.e. electronics and light enclosure. The time error is principally due to the thickness of the shower disk. However, near the shower core and for zenith angles less than 30° the inherent time error due to light enclosure and electronic circuits is more important than other errors. It is therefore concluded that, in order to achieve better angular resolutions, EAS experiments must be established along with tracking techniques (Bernlohr et al., 1996). The zenith angle of the arrival direction of air showers, obeys a $\cos^n \theta$ law with $n = 7.2 \pm 0.2$. On the other hand, when an air shower arrives at an angle to the earth's magnetic field, the charged particles in the cascade can be deflected. Ivanov et al. (1999) have formulated the effect of geomagnetic field on EAS. For showers arriving from the north the shower particles have higher deflection than the southern showers of the equal energy with the equal zenith angle. Thus, it gives the decrease of event rate as it is shown in Figures 9 and 10. The amplitudes

of the first two harmonics, can be fitted to $A_I \approx (0.02 + 0.35 \sin^2\theta) \pm 0.02$, and $A_{II} \approx (0.03 + 0.42 \sin^4\theta) \pm 0.03$.

Appendix

Calculation of the arrival direction of an air shower:
In the present analysis, the arrival direction of an air shower is determined assuming the shower front can be approximated by a plane:

$$z + a_1 x + b_1 y + c_1 = 0 \,,$$

where we take a coordinate system on the ground; x is east-west, y is north-south and z is vertical. c_1 is a constant related to the origin of the timing measurements. The zenith angle, θ, and the azimuth angle, ϕ, are related to shower front plane as follows:

$$\tan\theta = (a_1^2 + b_1^2)^{1/2}, \qquad \cos\theta = (1 + a_1^2 + b_1^2)^{-1/2} \,,$$
$$\cos\phi = a_1 (a_1^2 + b_1^2)^{-1/2}, \quad \sin\phi = b_1 (a_1^2 + b_1^2)^{-1/2} \,.$$

If we take (x_i, y_i, z_i) as the coordinates of the ith scintillator, the distance between each scintillator and the shower front is presented by:

$$l_i = (a_1 x_i + b_1 y_i + c_1 + z_i)(1 + a_1^2 + b_1^2)^{-1/2} \,.$$

If we take t_i as the time distance between shower front and ith scintillator after correction for the time delay in cable, and the time dispersions of the experimental instruments, the sum of the squares of the differences between $cT_{4j} = c(t_4 - t_j)$ and $l_{4j} = l_4 - l_j$ is given by $\sum_{j=1}^{3} (l_{4j} - cT_{4j})^2$, where c is the velocity of light, and the distances and times were measured with respect to the scintillator No. 4. If we introduce a new variables $\alpha_j = x_4 - x_j$, $\beta_j = y_4 - y_j$, $X = a_1(1 + a_1^2 + b_1^2)^{-1/2}$ and $Y = b_1(1 + a_1^2 + b_1^2)^{-1/2}$, the sum of squares of differences between cT_{4j} and l_{4j} becomes $\sum (\alpha_j X + \beta_j Y - cT_{4j})^2$, where we have assumed that all of scintillators are on xy plane ($z_i = 0$). By minimizing this summation with respect to X and Y we obtain

$$X = c \begin{vmatrix} \sum \alpha_j T_{4j} & \sum \alpha_j \beta_j \\ \sum \beta_j T_{4j} & \sum \beta_j^2 \end{vmatrix} \Bigg/ \begin{vmatrix} \sum \alpha_j^2 & \sum \alpha_j \beta_j \\ \sum \alpha_j \beta_j & \sum \beta_j^2 \end{vmatrix} ,$$

$$Y = c \begin{vmatrix} \sum \beta_j T_{4j} & \sum \alpha_j \beta_j \\ \sum \alpha_j T_{4j} & \sum \alpha_j^2 \end{vmatrix} \Bigg/ \begin{vmatrix} \sum \alpha_j^2 & \sum \alpha_j \beta_j \\ \sum \alpha_j \beta_j & \sum \beta_j^2 \end{vmatrix} .$$

Then by using the X and Y values, the zenith angle, θ, and azimuth angle, ϕ, are determined by:

$$\theta = \tan^{-1}\left(\sqrt{\frac{X^2+Y^2}{1-X^2-Y^2}}\right), \qquad \phi = \tan^{-1}(Y/X)\,.$$

Acknowledgements

This research has been partly supported by Grant No. NRCI 1853 of National Research Council of Islamic Republic of Iran. We are indebted to the anonymous referee for his numerous constructive comments.

References

Bahmanabadi, M. et al.: 1998, *Experimental Astronomy* **8**, 211.
Bernlohr, K. et al.: 1996, *NIM* **A369**(1), 284.
Bertou X. et al.: 2000, *Int. J. Mod. Phys.* **A15**, 2181−2224.
Heck, D. et al.: 1998, CORSIKA (Cosmic Ray Simulation for KASCADE) FZKA6019 (Forschungszentrum Karlsruhe).
http://www.ngdc.noaa.gov/seg/potfld/geomag.html, June 2002.
Ivanov, A. A. et al.: 1999, *JETP Lett.* **69**, 288−293.
Linsley, J.: 1986, *J. Phys. G. Nucl. Phys.* **12**, 51.
Luorui S. and Winn M. M.: 1984, *NIM* **A223**, 173.
Mitsui K. et al.: 1990, *NIM A290*, 565.
Nishizawa M. et al.: 1989, *NIM A285*, 532.